High-Speed Galvanostatic Anodizing without Oxide Burning using a Nanodimpled Aluminum Surface for Nanoporous Alumina Fabrication

Mana Iwai, Tatsuya Kikuchi*, Ryosuke O. Suzuki
Faculty of Engineering, Hokkaido University, N13-W8, Kita-ku, Sapporo, Hokkaido, 060-8628, Japan

*Corresponding author: Tatsuya Kikuchi
e-mail: kiku@eng.hokudai.ac.jp

Abstract

Rapid formation of a porous alumina film without oxide burning was achieved by anodizing in etidronic acid at large current densities using a nanodimpled aluminum surface. After the electropolished aluminum specimens were galvanostatically anodized in a 0.3 M etidronic acid solution at 293 K, a uniform porous alumina film without oxide burning was formed at relatively low current densities of up to 20 Am^{-2}. After the first anodizing process, an array of dimples was fabricated on the aluminum surface by oxide film removal in a chromic acid/phosphoric acid solution. After the nanostructured aluminum specimen was galvanostatically anodized once again under the same conditions, the possible applied current density without burning increased with the size of the nanodimples, and the current density during the high-speed anodizing process of the dimpled aluminum specimen increased by five times. Many pores grew on the whole surface of the aluminum dimples from the initial anodizing stage; then, pores that grew from the bottom of the dimples survived the anodizing process, and a clear porous alumina film was formed as the voltage reached the maximum value.

Keywords: Dimpled aluminum; Galvanostatic anodizing; Porous alumina; Oxide burning

1. Introduction

Electrochemical anodizing of aluminum in suitable acidic solutions produces a porous alumina coating that possesses a characteristic self-organized hexagonal nanostructure [1,2]. Various unique characteristics, such as an improved corrosion resistance [3-8], wear resistance [9], Vickers hardness [10-12], coloring [13-16], and self-ordering of a nanoporous structure [17-23], can be produced on the aluminum surface by anodizing. Galvanostatic anodizing is usually employed for industrial processes due to easy handling of the electric current and production of a porous alumina film, and a porous alumina film can be rapidly formed by anodizing at high current density conditions. However, excessive current densities during anodizing cause the nonuniform growth of porous alumina due to localized current concentrations (oxide burning) [24-29]. In particular, anodizing using phosphoric, etidronic, arsenic, citric, and malic acid solutions leads to relatively high voltages; thus, oxide burning is easily induced during anodizing [30-36]. Hence, a novel anodizing technique must be developed for rapid growth without oxide burning during anodizing at high voltages. A recently developed new technique known as “hard anodizing” enables the rapid fabrication of porous alumina films without burning [37-40]. However, this method requires special equipment with a powerful back-cooling unit, and the porous alumina coating is limited to a narrow surface area.

Two-step potentiostatic anodizing is widely used to fabricate highly ordered porous alumina structures from the top to the bottom [41,42]. In this method, potentiostatic anodizing under the appropriate conditions gradually leads to self-ordering of the pore distribution. As the porous alumina film is chemically removed from the substrate, a regularly arranged dimpled structure is obtained on the aluminum surface. Next, potentiostatic anodizing at the same applied voltage induces the formation of pores from the bottom of the ordered dimples; thus, an ordered porous alumina film can be obtained by potentiostatic anodizing twice and etching without any complicated equipment. In the present investigation, we show that this two-step anodizing method can be applicable to high current density galvanostatic anodizing for the rapid formation of porous alumina films without oxide burning. We found that the largest possible current density that can be applied without oxide burning greatly increases by galvanostatic anodizing an aluminum specimen with an array of dimples. The electrochemical behavior and the resulting porous alumina film obtained by the first and second galvanostatic anodizing processes were investigated in detail.

2. Experimental

Commercially available 5N aluminum sheets measuring 500 μm in thickness (Nippon Light Metal, Japan) were used for anodizing the materials. The aluminum sheets were cut into square pieces with dimensions of 20 mm × 20 mm with a slight electrical connection part, and then ultrasonic cleaning was carried out in ethanol for 10 min. The bottom half of the connection part was covered with a silicone resin (KE45W, Shin-Etsu Silicone, Japan) to isolate the reaction area. The specimens were electropolished at a constant voltage of 28 V in CH_3COOH (78 vol%)/70%-$HClO_4$ (22 vol%) at 280 K for 1 min.

The pretreated aluminum specimens were anodized in a 0.3 M etidronic acid solution (TCI, Japan) [31-33,43-46]. A typical simple electrochemical cell was used for anodizing, and a schematic of the apparatus is shown in Figure 1. A 150 mL aliquot of etidronic acid solution was added to the

glass cell with a 55 mm inner diameter. An aluminum anode was immersed in the solution at the center of the glass cell, and a platinum cathode was placed in parallel 22 mm from the anode. The electrochemical cell was placed in a large constant temperature bath (UCT-1000A, AS ONE, Japan), and the temperature of the etidronic acid solution was maintained at 293 K. The etidronic acid solution was stirred at a rotating speed of 250 rpm using an underwater magnetic mixer (HP40175, ISIS Co., Japan). The aluminum specimens were galvanostatically anodized at 5.0-100 Am^{-2} using a direct current power supply system (PWR400H, Kikusui Electronics, Japan) for 2 h (first anodizing process). A digital multimeter (VOAC7602, IWATSU, Japan) was used for the measurements of the voltage-time curves during anodizing. After the first anodizing process, the porous alumina film was chemically dissolved in a 0.20 M CrO_3/0.51 M H_3PO_4 solution at 353 K, and nanoscale dimples were exposed on the surface. The nanostructured aluminum specimens were galvanostatically anodized once again from 5.0-120 Am^{-2} for 2 h (second anodizing process). The aluminum specimens were also anodized at 20-100 Am^{-2} and 293 K in a 0.3 M phosphoric acid solution for 60 min to examine the applicability of high-speed galvanostatic anodizing using the nanodimpled aluminum surface.

To examine the effect of the depth of the aluminum dimples on the anodizing behavior, several dimple structures with different depths were fabricated by the following procedures before the second anodizing process; the nanodimpled aluminum specimens were anodized at 10 Am^{-2} in a 0.5 M H_3BO_4/0.05 M $Na_2B_4O_7$ at 293 K to grow a thin barrier oxide film, and then the oxide film was chemically dissolved (i.e., smoothening occurred).

The surface morphology of the anodized specimens was observed by atomic force microscopy (AFM: Nanocute, Hitachi High-Technologies, Japan) and scanning electron microscopy (SEM: JSM6500F, JEOL, Japan, and TM-1000, Hitachi High-Technologies). The initial growth behavior of the porous alumina film was observed by spherical aberration-corrected scanning transmission electron microscopy (Cs-corrected STEM: Titan3 G2 60–300, FEI, USA). The method for the preparation of STEM specimens is described elsewhere [33]. The anion distribution in the anodic oxide was studied by energy dispersive X-ray spectrometry (EDS).

3. Results and Discussion

Figure 2a represents the voltage (U_1) – time (t_1) curves measured during the first galvanostatic anodizing process of the electropolished aluminum in a 0.3 M etidronic acid solution at 293 K for 120 min. The anodizing voltage exhibited a plateau value after the initial fluctuation at a low current density range from i_1 = 5.0–20.0 Am^{-2}, and these U_1-t_1 curves can be typically obtained by the steady-state growth of a porous alumina film during anodizing [2,47]. The surface appearance of the specimen anodized at i_1 = 20.0 Am^{-2} is shown in the inset of Fig. 1a, and the aluminum surface was completely covered with a uniform light grayish oxide film without any defects. However, the voltage suddenly dropped before it reached the largest value at the elevated current density of i_1 = 40.0 Am^{-2}, and the decrease curve before reaching the plateau voltage was not smooth. Accordingly, a nonuniform dark grayish oxide film was formed on the surface under the silicone resin (white arrow shown in the inset). This unstable voltage change and the corresponding nonuniform oxide formation became more intense as the current density increased to i_1 = 100 Am^{-2}; thus, most of the

surface was covered with a nonuniform dark grayish oxide (inset figure). Figure 2b shows SEM images of the surface of the uniform light grayish oxide formed at i_1 = 20.0 Am^{-2} and the nonuniform dark grayish oxide formed at 40.0 Am^{-2}. A typical porous alumina film with black nanoscale pores was observed on the uniform light grayish oxide film formed at i_1 = 20.0 Am^{-2}. However, many humpy regions and subsequent cracks were formed on the nonuniform dark grayish oxide formed at 40.0 Am^{-2}; although similar nanopores were observed in the high-magnification image, the oxide film with many defects was caused by burning at an increased current density. Therefore, the application of excessive current densities during anodizing at high voltages should usually be avoided for the coating of uniform porous alumina films. Thus, two-step galvanostatic anodizing is a useful method for the rapid formation of porous alumina films without oxide burning, as described below.

After a stable first anodizing process without burning at i_1 = 5.0 Am^{-2} and 10.0 Am^{-2} for 120 min, the obtained porous film was completely dissolved in a chlomic acid and phosphoric acid solution, and then a dimple structure was obtained on the aluminum surface. Figure 3 shows the three-dimensional AFM images of the electropolished aluminum and the nanostructured surfaces. Numerous small dimples measuring approximately 105 nm in average diameter and 3 nm in depth were formed by electropolishing the aluminum (Fig. 3a). After anodizing at i_1 = 5.0 Am^{-2} and removing the oxide (Fig. 3b), a larger dimple distribution measuring 285 nm in diameter and 310 nm in depth was obtained on the surface due to the formation of hemispherical barrier oxide at the bottom of the porous alumina film. The diameter and depth of the dimples formed at i_1 = 10.0 Am^{-2} increased to 387 nm and 495 nm, respectively, because the cell size of the porous layer increased with the voltage during galvanostatic anodizing. These nanodimpled aluminum specimens were galvanostatically anodized once again to determine the anodizing behavior.

Figure 4 represents the voltage (U_2) – time (t_2) curves obtained by the second galvanostatic anodizing process using the smaller nanodimpled specimen (i_1 = 5.0 Am^{-2}) under the same anodizing conditions shown in Fig. 2a. Characteristically, the height of the initial voltage peaks before the plateau value was smaller than that obtained by the first galvanostatic anodizing process. A stable formation of porous alumina films without burning could be achieved up to i_2 = 40.0 Am^{-2} during the second galvanostatic anodizing process by using the nanodimpled specimen. However, the anodizing voltage suddenly decreased at a larger current density of i_1 = 60.0 Am^{-2} due to burning, and a consequent nonuniform dark grayish oxide was formed on the surface (white arrow). Thus, the largest current density without oxide burning increased to i_2 = 40.0 Am^{-2} (Fig. 4) from i_1 = 20.0 Am^{-2} (Fig. 2a) under the same conditions, and rapid formation of a porous alumina film could be realized using nanodimpled aluminum instead of conventional flat aluminum.

The effect of the average size of the dimples on the anodizing behavior was investigated. The U_2–t_2 curves obtained by the second galvanostatic anodizing process using the larger nanodimpled specimen (i_2 = 10.0 Am^{-2}) is shown in Figure 5. A stable anodizing process without oxide burning could be achieved at up to i_2 = 100.0 Am^{-2}, and uniform porous alumina films were successfully obtained. However, a sudden decrease and subsequent unstable fluctuating behavior of the voltage were measured at 120.0 Am^{-2}, and a nonuniform oxide film was obtained on the surface. Therefore, the largest current density without oxide burning increased with the size of the nanodimples formed

on the aluminum surface. Based on the experimental results obtained by the second galvanostatic anodizing process, high-current-density anodizing without burning can be achieved using the aluminum specimen covered with the larger dimples.

Figure 6 summarizes the dependence of the current densities during the first and second anodizing processes on the oxide burning phenomenon. In this domain diagram, the circles represent the formation of a uniform porous alumina film without burning, whereas the crosses represent the formation of a nonuniform oxide film with many cracks by burning. After the electropolished aluminum was galvanostatically anodized in etidronic acid solution, uniform porous alumina formation without burning occurred at current densities less than 20 Am^{-2}. The largest current density obtained by the second anodizing process gradually increased with the current density during the first anodizing process; in other words, it was related to the size of the dimples. As a result, the applicable current density without oxide burning can be two and five times larger than that of the electropolished aluminum, and rapid formation of the porous alumina film can be achieved by using the nanodimpled aluminum surface.

To investigate the effect of the nanodimpled structure on the anodizing behavior, nanodimpled aluminum specimens with different depths were anodized under the same conditions. The nanodimpled aluminum fabricated by the first anodizing process at i_1 = 10 Am^{-2} was galvanostatically anodized at up to 300 V in a neutral borate solution to form a barrier oxide film on the dimple structure. Because barrier oxide formation leads to the gradual smoothing of the growth interface of the oxide film during anodizing [48], dimples with a smaller depth but the same diameter can be fabricated on the surface after barrier oxide dissolution from the aluminum substrate (i.e., shallow dimples). Figure 7a illustrates a three-dimensional AFM image of the aluminum dimple structure fabricated by barrier oxide formation and subsequent oxide removal. The deep dimples shown in Fig. 2c disappeared by this smoothing process, and shallow dimples were obtained on the aluminum surface. Figure 7b shows the *U–t* curves obtained by galvanostatic anodizing at i_1 = 10 Am^{-2} using the electropolished aluminum and deep/shallow dimples. Here, the surface roughness of these specimens obtained by AFM measurements, Ra, was measured to be 0.8 nm (electropolished), 54.0 nm (deep), and 11.8 nm (shallow). The plateau voltages after the initial transient exhibited almost the same value of approximately 156 V, whereas the slope of the initial linear increase obtained with the deep dimples was smaller than that of the electropolished aluminum and shallow dimples due to their large surface area. Regarding the initial voltage peaks during anodizing, the peak values decreased with the surface roughness and the dimple depth: 229 V with the electropolished aluminum, 200 V with the shallow dimples, and 165 V with the deep dimples. Therefore, the initial linear voltage increase during anodizing at the same current density was suppressed via the formation of deep dimples on the aluminum surface. The excess voltage during galvanostatic anodizing caused their sudden decrease and subsequent oxide burning (Figs. 2, 4, and 5). The suppression effect of the initial voltage increase on the nanodimpled aluminum enabled the subsequent rapid, stable formation of the porous alumina film without oxide burning at high current densities. The reason that the nanodimpled surface suppresses voltage increase during galvanostatic anodizing may be due to the rapid inducing of the pore formation at the bottom of dimples.

Figures 8a-8c represent the growth behavior of the porous alumina film on the nanodimpled

aluminum surface during the second galvanostatic anodizing process at i_2 = 5 Am^{-2} for a) t_2 = 10 min, b) 20 min, and c) 29 min. Here, the dimple structure was formed by the first anodizing process at the same current density of i_1 = 5 Am^{-2}. When the nanodimpled aluminum was anodized for up to 10 min (Fig. 8a), a thin oxide film measuring approximately 70 nm in thickness was uniformly formed along the hemispherical curvature surface. Although this anodizing time corresponds to the middle stage of the linear voltage increase on the U_2-t_2 curve shown in Fig. 8f, many small pores with a size of approximately 10 nm were already formed on the top surface of the alumina film (see high-magnification TEM image in Fig. 8d). This early pore formation behavior was also observed using the electropolished flat surface [33]. As the anodizing time increased to t_2 = 20 min, the thickness of the bottom dense alumina layer increased in thickness due to a voltage increase, and larger pores were clearly observed on the outer surface (Fig. 8b). It can be seen that the size of these pores gradually increased towards the bottom from the top of the dimples (i.e., from b4 to b1, as shown with the white arrows). Figure 8e shows an elemental mapping image of the oxygen (blue) and phosphorus (yellow) distribution in the porous alumina film formed for t_2 = 20 min. Etidronate containing two phosphorus atoms was incorporated into the aluminum oxide from the bottom of the pores during galvanostatic anodizing. The thickness of the phosphorus-incorporated layer gradually increased towards the bottom from the top of the dimples (i.e., from e3 to e1, as shown with the white arrows). The nanopores formed on the dimple walls hit with other pores grown from neighboring dimples, and then, they stopped growing (e2 and e3). Therefore, the pores grown from the bottom of the dimples survived the anodizing process, and a porous alumina film with a clear cell structure and a large pore at the bottom was formed at the largest voltage for t_2 = 29 min (Fig. 8c).

This high-speed galvanostatic anodizing method using the nanodimpled aluminum surface is also useful for other high-voltage acidic electrolyte, such as phosphoric acid. Phosphoric acid is well-known as a typical electrolyte for the fabrication of porous alumina films with a large-scale cell size at high voltages [49,50]. Figure 9a represents the voltage (U_1) – time (t_1) curves measured during the first galvanostatic anodizing process of the electropolished aluminum in a 0.3 M phosphoric acid solution at 293 K for 20 min. Sudden decreases and subsequent unstable fluctuating behaviors of the voltage were measured at 60-100 Am^{-2} during first galvanostatic anodizing, and a nonuniform oxide film with many cracks was formed on the surface. However, as the nanodimpled aluminum specimen fabricated via first anodizing at 20 Am^{-2} for 60 min was anodized under the same conditions (second galvanostatic anodizing, Fig. 9b), a stable formation of porous alumina films without burning could be successfully achieved at higher current densities of 60-100 Am^{-2}. Therefore, the possible applied current density without oxide burning can increase using the nanodimpled aluminum surface during galvanostatic anodizing under high-voltage conditions.

In summary, we described the rapid formation of a porous alumina film without oxide burning by using nanodimpled aluminum, and this method is useful for the high-speed anodizing process in various industrial applications. However, the process is slightly more complicated than the simple anodizing technique because it involves extra processes, including a first anodizing process and oxide dissolution, to form dimples on the aluminum surface. This issue may be improved by surface texturing of the dimples on an aluminum plate before anodizing; specifically, dimples can be fabricated by nanoimprinting using a rolling mill roll with a nanoconvex structure during the rolling

process of an aluminum plate, and then the nanostructured aluminum can be anodized at larger current densities without oxide burning.

4. Conclusions

High-speed anodizing in etidronic acid without oxide burning becomes possible when a nanodimpled aluminum surface is used. Stable galvanostatic anodizing of an electropolished aluminum specimen in a 0.3 M etidronic acid solution at 293 K is only achieved at a current density of up to 20 Am^{-2}, and a higher current density increase leads to burning. The peak voltage measured at the early stage of galvanostatic anodizing decreases by using the nanodimpled aluminum specimen, and the possible applied current density without burning increases with the current density during the first anodizing process and the corresponding size of the nanodimpled structure. As a result, current densities that are increased by two times (40 Am^{-2}) and five times (100 Am^{-2}) can be applied to the dimpled aluminum specimen formed by first anodizing process at 5 Am^{-2} and 10 Am^{-2}, respectively. Many pores grow on the whole surface of the aluminum dimple structure from the initial anodizing stage, whereas the pores grown from the bottom of the dimples survive eventually during anodizing, and a clear porous alumina film is formed as the voltage reaches the maximum value.

Acknowledgments

This study was funded by the Light Metal Educational Foundation, the Japan Society for the Promotion of Science KAKENHI (19H02470), and the Hokkaido University Nanotechnology Platform Program of the Ministry of Education, Culture, Sports, Science and Technology (A-19-HK-0034 and A-20-HK-0037). We are also thankful to Mr. Ryo Oota, Mr. Nobuyuki Miyazaki, and Dr. Takashi Endo for their help with the STEM and SEM observations.

References

1) H. Masuda, K. Fukuda, Ordered metal nanohole arrays made by a two-step replication of honeycomb structures of anodic alumina, Science 268 (1995) 1466-1468. https://doi.org/10.1126/science.268.5216.1466
2) W. Lee, D. J. Park, Porous anodic aluminum oxide: anodization and templated synthesis of functional nanostructures, Chem. Rev., 114 (2014) 7487-7556. https://doi.org/10.1021/cr500002z
3) T. Aerts, T. Dimogerontakis, I.D. Graeve, J. Fransaer, H. Terryn, Influence of the anodizing temperature on the porosity and the mechanical properties of the porous anodic oxide film, Surf. Coat. Technol. 201 (2007) 7310-7317. https://doi.org/10.1016/j.surfcoat.2007.01.044
4) T. He, Y. Wang, Y. Zhang, T. Xu, T. Liu, Super-hydrophobic surface treatment as corrosion protection for aluminum in seawater, Corr. Sci. 51 (2009) 1757-1761. https://doi.org/10.1016/j.corsci.2009.04.027
5) V.R. Capelossi, M. Poelman, I. Recloux, R.P.B. Hernandez, H.G.D. Melo, M.G. Olivier, Corrosion protection of clad 2024 aluminum alloy anodized in tartaric-sulfuric acid bath and protected with hybrid sol–gel coating, Electrochim. Acta 124 (2014) 69-79. https://doi.org/10.1016/j.electacta.2013.09.004

6) M. Curioni, P. Skeldon, E. Koroleva, G.E. Thompson, J. Ferguson, Role of tartaric acid on the anodizing and corrosion behavior of AA 2024 T3 aluminum alloy, J. Electrochem. Soc. 156 (2009) C147-C153. https://doi.org/10.1149/1.3077602
7) Y. Suzuki, K. Kawahara, T. Kikuchi, R. O. Suzuki, S. Natsui, Corrosion-resistant porous alumina formed via anodizing aluminum in etidronic acid and its pore-sealing behavior in boiling water, J. Electrochem. Soc. 166 (2019) C261-C269. https://doi.org/10.1149/2.0221912jes
8) T. Kikuchi, Y. Suzuki, M. Iwai, R.O. Suzuki, Anodizing aluminum and its alloys in etidronic acid to enhance their corrosion resistance in a sodium chloride solution, J. Electrochem. Soc. accepted manuscript, available online. https://doi.org/10.1149/1945-7111/abaa6b
9) L. Benea, V. Dumitrascu, Enhancement in sustained friction and wear resistance of nanoporous aluminum oxide films obtained by controlled electrochemical oxidation process. RSC Adv. 9 (2019) 25056-25063. https://doi.org/10.1039/C9RA05702A
10) D.R. Gabe, Hard anodizing—What do we mean by hard?, Metal Finishing 100 (2002) 52-58. https://doi.org/10.1016/S0026-0576(02)80936-9
11) T. Kikuchi, A. Takenaga, S. Natsui, R.O. Suzuki, Advanced hard anodic alumina coatings via etidronic acid anodizing, Surf. Coat. Technol. 326 (2017) 72-78. https://doi.org/10.1016/j.surfcoat.2017.07.043
12) M. Kim, H. Yoo, J. Choi, Non-nickel-based sealing of anodic porous aluminum oxide in $NaAlO_2$, Surf. Coat. Technol. 310 (2017) 106-112. https://doi.org/10.1016/j.surfcoat.2016.11.100
13) Y. Liu, Y. Chang, Z. Ling, X. Hu, Y. Li, Structural coloring of aluminum, Electrochem Commun. 12 (2011) 1336-1339. https://doi.org/10.1016/j.elecom.2011.08.008
14) J. Martín, M. Martín-González, J.F. Fernández, O. Caballero-Calero, Ordered three-dimensional interconnected nanoarchitectures in anodic porous alumina, Nat. Commun. 5 (2014) 1-9. https://doi.org/10.1038/ncomms6130
15) T. Kikuchi, O. Nishinaga, S. Natsui, R. O. Suzuki, Polymer nanoimprinting using an anodized aluminum mold for structural coloration, Appl. Surf. Sci. 341 (2015) 19-27. https://doi.org/10.1016/j.apsusc.2015.03.007
16) H. Segawa, K. Wada, Structural colors of laminated alumina films prepared by ac oxidation in oxalic acid solution, Mater. Chem. Phys. 250 (2020) 123031. https://doi.org/10.1016/j.matchemphys.2020.123031
17) M.A. Kashi, A. Ramazani, M. Raoufi, A. Karimzadeh, Self-ordering of anodic nanoporous alumina fabricated by accelerated mild anodization method, Thin Solid Films 518 (2010) 6767-6772. https://doi.org/10.1016/j.tsf.2010.06.020
18) H. Masuda, F. Matsumoto, K. Nishio, Fabrication of functional devices based on highly ordered anodic porous alumina, Electrochemistry 72 (2004) 389-394. https://doi.org/10.5796/electrochemistry.72.389
19) H. Asoh, K. Nishio, M. Nakao, T. Tamamura, H. Masuda, Conditions for fabrication of ideally ordered anodic porous alumina using pretextured Al, J. Electrochem. Soc. 148 (2001) B152-B156. https://doi.org/10.1149/1.1355686
20) H. Masuda, H. Asoh, M. Watanabe, K. Nishio, M. Nakao, T. Tamamura, Square and triangular nanohole array architectures in anodic alumina, Adv. Mater. 13 (2001) 189-192.

https://doi.org/10.1002/1521-4095(200102)13:3<189::AID-ADMA189>3.0.CO;2-Z
21) S.Z. Kure-Chu, K. Osaka, H. Yashiro, H. Segawa, K. Wada, S. Inoue, Controllable fabrication of networked three-dimensional nanoporous anodic alumina films on low-purity Al materials, J. Electrochem. Soc. 162 (2014) C24-C34. https://doi.org/10.1149/2.0511501jes
22) S.Z. Kure-Chu, K. Osaka, H. Yashiro, K. Wada, H. Segawa, S. Inoue, Facile Fabrication of Ordered Multi-Tiered Hierarchical Porous Alumina Nanostructures with Multiple and Fractional Ratios of Pore Interval toward Multifunctional Nanomaterials, ECS J. Solid State Sci. Technol. 5 (2016) P285-P292. https://doi.org/10.1149/2.0231605jss
23) M. A. Kashi, A. Ramazani, H. Abbasian, A. Khayyatian, Capacitive humidity sensors based on large diameter porous alumina prepared by high current anodization, Sens. Actuator A Phys. 174 (2012) 69-74. https://doi.org/10.1016/j.sna.2011.11.033
24) S. Ono, M. Saito, H. Asoh, Self-ordering of anodic porous alumina induced by local current concentration: burning, Electrochem. Solid State Lett. 7 (2004) B21-B24. https://doi.org/10.1149/1.1738553
25) S. Ono, M. Saito, M. Ishiguro, H. Asoh, Controlling factor of self-ordering of anodic porous alumina, J. Electrochem. Soc. 151 (2004) B473-B478. https://doi.org/10.1149/1.1767838
26) S. Ono, M. Saito, H. Asoh, Self-ordering of anodic porous alumina formed in organic acid electrolytes, Electrochim. Acta 51 (2005) 827-833. https://doi.org/10.1016/j.electacta.2005.05.058
27) B. Gastón-García, E. García-Lecina, J. A. Díez, M. Belenguer, C. Müller, Local burning phenomena in sulfuric acid anodizing: analysis of porous anodic alumina layers on AA1050, Electrochem. Solid State Lett. 13 (2010) C33-C35. https://doi.org/10.1149/1.3478482
28) T. Aerts, I.D. Graeve, H. Terryn, Study of initiation and development of local burning phenomena during anodizing of aluminium under controlled convection, Electrochim. Acta 54 (2008) 270-279. https://doi.org/10.1016/j.electacta.2008.08.004
29) C. Lämmel, M. Schneider, C. Heubner, W. Beckert, A. Michaelis, Investigations of burning phenomena during the hard anodising of aluminium by local in-operando temperature measurements. Electrochim. Acta 249 (2017) 271-277. https://doi.org/10.1016/j.electacta.2017.07.167
30) L. Zaraska, G.D. Sulka, M. Jaskuła, The effect of n-alcohols on porous anodic alumina formed by self-organized two-step anodizing of aluminum in phosphoric acid, Surf. Coat. Technol. 204 (2010) 1729-1737. https://doi.org/10.1016/j.surfcoat.2009.10.051
31) T. Kikuchi, O. Nishinaga, S. Natsui, R.O. Suzuki, Fabrication of self-ordered porous alumina via etidronic acid anodizing and structural color generation from submicrometer-scale dimple array, Electrochim. Acta 156 (2015) 235-243. https://doi.org/10.1016/j.electacta.2014.12.171
32) M. Iwai, T. Kikuchi, R.O. Suzuki, Electrochemical and morphological characterization of porous alumina formed by galvanostatic anodizing in etidronic acid, Electrochim. Acta 320 (2019) 134606. https://doi.org/10.1016/j.electacta.2019.134606
33) M. Iwai, T. Kikuchi, R.O. Suzuki, Initial Structural Changes of Porous Alumina Film via High-Resolution Microscopy Observations, ECS J. Solid State Sci. Technol. 9 (2020) 044004. https://orcid.org/0000-0003-1543-6256

34) S. Akiya, T. Kikuchi, S. Natsui, R.O. Suzuki, Nanostructural characterization of large-scale porous alumina fabricated via anodizing in arsenic acid solution, Appl. Surf. Sci. 403 (2017) 652-661. https://doi.org/10.1016/j.apsusc.2017.01.243
35) S.Z. Chu, K. Wada, S. Inoue, M. Isogai, Y. Katsuta, A. Yasumori, Large-scale fabrication of ordered nanoporous alumina films with arbitrary pore intervals by critical-potential anodization, J. Electrochem. Soc. 153 (2006) B384-B391. https://doi.org/10.1149/1.2218822
36) T. Kikuchi, T. Yamamoto, R.O. Suzuki, Growth behavior of anodic porous alumina formed in malic acid solution, Appl. Surf. Sci. 284 (2013) 907-913. https://doi.org/10.1149/1.2218822
37) W. Lee, R. Ji, U. Gösele, K. Nielsch, Fast fabrication of long-range ordered porous alumina membranes by hard anodization, Nat. Mater. 5 (2006) 741-747. https://doi.org/10.1038/nmat1717
38) K. Schwirn, W. Lee, R. Hillebrand, M. Steinhart, K. Nielsch, U. Gösele, Self-ordered anodic aluminum oxide formed by H_2SO_4 hard anodization, ACS Nano 2 (2008) 302-310. https://doi.org/10.1021/nn7001322
39) W. Lee, J. C. Kim, U. Gösele, Spontaneous current oscillations during hard anodization of aluminum under potentiostatic conditions, Adv. Funct. Mater. 20 (2010) 21-27. https://doi.org/10.1002/adfm.200901213
40) M. Norek, M. Dopierała, W.J. Stępniowski, Ethanol influence on arrangement and geometrical parameters of aluminum concaves prepared in a modified hard anodization for fabrication of highly ordered nanoporous alumina, J. Electroanal. Chem. 750 (2015) 79-88. https://doi.org/10.1016/j.jelechem.2015.05.024
41) J.M. Montero-Moreno, M. Sarret, C. Müller, Influence of the aluminum surface on the final results of a two-step anodizing, Surf. Coat. Technol. 201 (2007) 6352-6357. https://doi.org/10.1016/j.surfcoat.2006.12.003
42) X.Y. Han, W.Z. Shen, Improved two-step anodization technique for ordered porous anodic aluminum membranes, J. Electroanal. Chem. 655 (2011) 56-64. https://doi.org/10.1016/j.jelechem.2011.02.008
43) A. Takenaga, T. Kikuchi, S. Natsui, R.O. Suzuki, Exploration for the self-ordering of porous alumina fabricated via anodizing in etidronic acid, Electrochim. Acta 211 (2016) 515-523. https://doi.org/10.1016/j.electacta.2016.06.071
44) M. Sepúlveda, J.G. Castaño, F. Echeverría, Influence of temperature and time on the fabrication of self-ordering porous alumina by anodizing in etidronic acid, Appl. Surf. Sci. 454 (2018) 210-217. https://doi.org/10.1016/j.apsusc.2018.05.081
45) T. Kikuchi, S. Akiya, K. Kunimoto, R. O. Suzuki, S. Natsui, Photoluminescence from Anodic Aluminum Oxide Formed via Etidronic Acid Anodizing and Enhancing the Intensity, Mater. Trans. 61 (2020) 1130-1137. https://doi.org/10.2320/matertrans.MT-M2020010
46) H. Huang, J. Qiu, M. Sun, W. Liu, X. Wei, Morphological evolution and burning behavior of oxide coating fabricated on aluminum immersed in etidronic acid at high current density, Surf. Coat. Technol. 374 (2019) 83-94. https://doi.org/10.1016/j.surfcoat.2019.05.081
47) G.E. Thompson, Porous anodic alumina: fabrication, characterization and applications, Thin Solid Films 297 (1997) 192-201. https://doi.org/10.1016/S0040-6090(96)09440-0
48) K. Shimizu, H. Habazaki, P. Skeldon, G.E. Thompson, G.C. Wood, Non-uniform sputtering and

degradation of depth resolution during GDOES depth profiling analysis of thin anodic alumina films grown over rough substrates, Surf. Interface Anal. 27 (1999) 950-954. https://doi.org/10.1002/(SICI)1096-9918(199910)27:10<950::AID-SIA658>3.0.CO;2-X

49) H. Masuda, K. Yada, A. Osaka, Self-ordering of cell configuration of anodic porous alumina with large-size pores in phosphoric acid solution, Jpn. J. Appl. Phys. 37 (1998) L1340. https://doi.org/10.1143/JJAP.37.L1340

50) L. Zaraska, G.D. Sulka, M. Jaskuła, The effect of n-alcohols on porous anodic alumina formed by self-organized two-step anodizing of aluminum in phosphoric acid, Surf. Coat. Technol. 204 (2010) 1729-1737. https://doi.org/10.1016/j.surfcoat.2009.10.051

Figure Captions

Figure 1 Schematic illustration of the two-electrode electrochemical anodizing cell.

Figure 2 a) Voltage (U_1) – time (t_1) curves measured by galvanostatic anodizing of the electropolished aluminum in a 0.3 M etidronic acid solution at 293 K for 120 min. b) Low- and high-magnification SEM images of the specimens anodized for 120 min at 20 Am^{-2} and 40 Am^{-2}.

Figure 3 Three-dimensional AFM images of the electropolished aluminum and the nanostructured dimple surfaces. The dimples were fabricated by anodizing at b) 5 Am^{-2} and c) 10 Am^{-2} and subsequent oxide removal.

Figure 4 Voltage (U_2) – time (t_2) curves measured during the second galvanostatic anodizing process of the nanostructured aluminum in a 0.3 M etidronic acid solution at 293 K for 120 min. The dimple structure was fabricated by the first galvanostatic anodizing process at 5 Am^{-2} and subsequent oxide removal.

Figure 5 Voltage (U_2) – time (t_2) curves measured during the second galvanostatic anodizing process of the nanostructured aluminum in a 0.3 M etidronic acid solution at 293 K for 120 min. Large dimples were fabricated by the first galvanostatic anodizing process at 10 Am^{-2} and subsequent oxide removal.

Figure 6 Domain diagram of oxide burning as a function of the current densities during the 1st and 2nd anodizing processes.

Figure 7 a) An AFM image of the shallow dimples fabricated by barrier oxide formation at 300 V and subsequent oxide removal. b) Voltage (U) – time (t) curves measured by galvanostatic anodizing of the a) electropolished aluminum, b) shallow dimples, and c) deep dimples in a 0.3 M etidronic acid solution at 293 K for 60 min.

Figure 8 a)-d) TEM images of the oxide film formed by the second galvanostatic anodizing process at 5 Am^{-2} for a) and d) 10 min, b) 20 min, and c) 29 min. The dimple structure was fabricated by the first galvanostatic anodizing process at 5 Am^{-2} and subsequent oxide removal. e) Elemental distribution maps of oxygen (blue) and phosphorus (yellow) in the anodic oxide formed by anodizing for 20 min. f) Voltage (U_2) – time (t_2) curves measured during the second galvanostatic anodizing process.

Figure 9 a) Voltage (U_1) – time (t_1) curves measured by first galvanostatic anodizing in a 0.3 M phosphoric acid solution at 293 K for 20 min. b) Voltage (U_2) – time (t_2) curves measured by second galvanostatic anodizing under the same conditions using the nanodimpled aluminum surface (i_1 = 20 Am^{-2}, t_1 = 60 min).

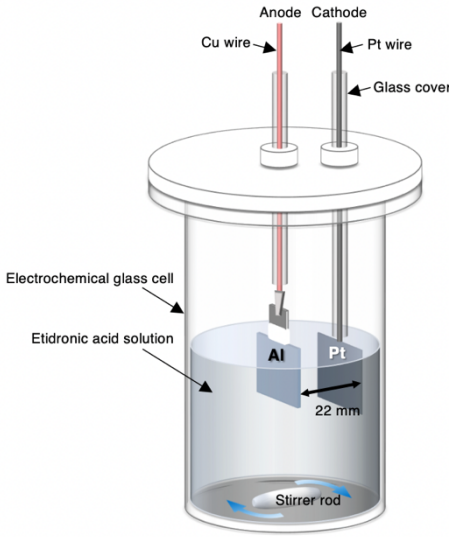
Anode
Cathode
Cu wire
Pt wire
Glass cover
Electrochemical glass cell
Etidronic acid solution
Al
Pt
22 mm
Stirrer rod

Figure 1.

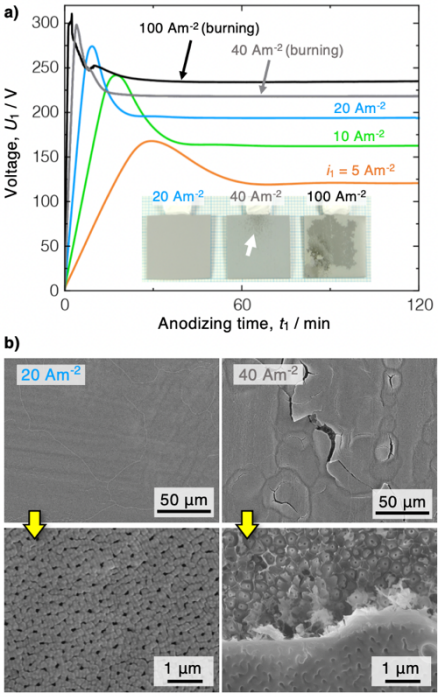
a)
100 Am-2 (burning)
40 Am-2 (burning)
20 Am-2
10 Am-2
i1 = 5 Am-2
20 Am-2
40 Am-2
100 Am-2
Voltage, U1 / V
Anodizing time, t1 / min
b)
20 Am-2
40 Am-2
50 µm
50 µm
1 µm
1 µm

Figure 2.

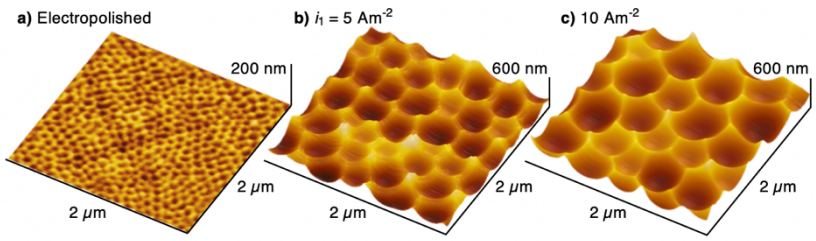
a) Electropolished
200 nm
2 μm
2 μm
b) i_1 = 5 Am^{-2}
600 nm
2 μm
2 μm
c) 10 Am^{-2}
600 nm
2 μm
2 μm

Figure 3.

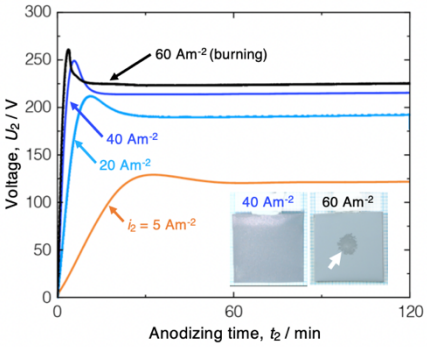
300
250
200
150
100
50
0
Voltage, U_2 / V
0
60
120
Anodizing time, t_2 / min
60 Am^{-2} (burning)
40 Am^{-2}
20 Am^{-2}
i_2 = 5 Am^{-2}
40 Am^{-2}
60 Am^{-2}

Figure 4.

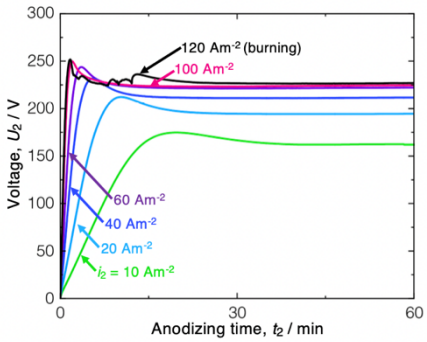
300
250
200
150
100
50
0
Voltage, U_2 / V
0
30
60
Anodizing time, t_2 / min
120 Am^{-2} (burning)
100 Am^{-2}
60 Am^{-2}
40 Am^{-2}
20 Am^{-2}
i_2 = 10 Am^{-2}

Figure 5.

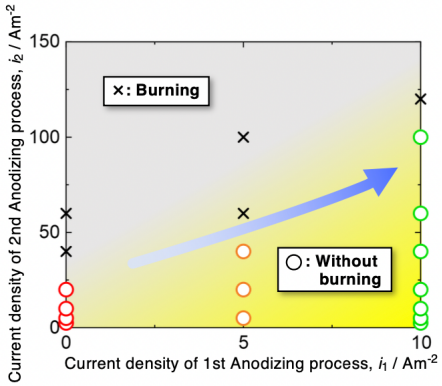
×: Burning
○: Without burning
Current density of 2nd Anodizing process, i_2 / Am^{-2}
Current density of 1st Anodizing process, i_1 / Am^{-2}
150
100
50
0
0
5
10

Figure 6.

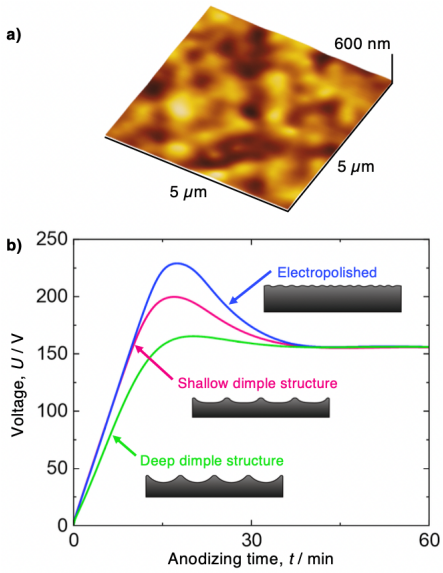
a)
600 nm
5 μm
5 μm
b)
250
200
150
100
50
0
Voltage, U / V
Electropolished
Shallow dimple structure
Deep dimple structure
0
30
60
Anodizing time, t / min

Figure 7.

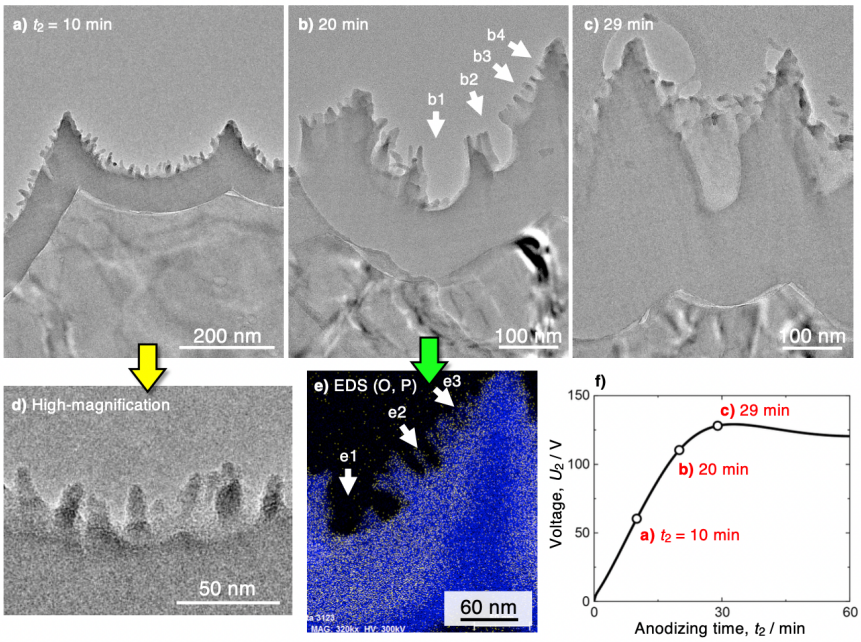
a) t_2 = 10 min
200 nm
b) 20 min
b1
b2
b3
b4
100 nm
c) 29 min
100 nm
d) High-magnification
50 nm
e) EDS (O, P)
e1
e2
e3
60 nm
f)
c) 29 min
b) 20 min
a) t_2 = 10 min
Voltage, U_2 / V
Anodizing time, t_2 / min
0
50
100
150
0
30
60

Figure 8.

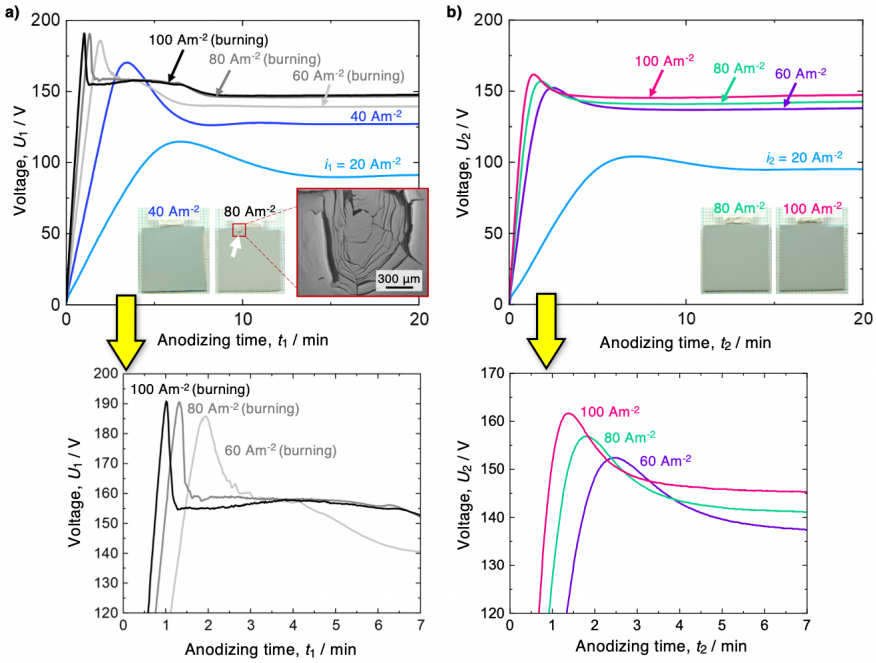
a)
b)
100 Am-2 (burning)
80 Am-2 (burning)
60 Am-2 (burning)
40 Am-2
i1 = 20 Am-2
i2 = 20 Am-2
300 μm
Voltage, U1 / V
Voltage, U2 / V
Anodizing time, t1 / min
Anodizing time, t2 / min

Figure 9.